Thermodynamic Characterization of the Redox Centers within Dimethylsulfide Dehydrogenase[†]

Nicole L. Creevey,[‡] Alastair G. McEwan,[‡] Graeme R. Hanson,[§] and Paul V. Bernhardt*[,‡]

School of Molecular and Microbial Sciences and Centre for Metals in Biology, Centre for Magnetic Resonance, University of Queensland, Brisbane 4072, Australia

Received December 14, 2007; Revised Manuscript Received January 30, 2008

ABSTRACT: Dimethylsulfide (DMS) dehydrogenase is a complex heterotrimeric enzyme that catalyzes the oxidation of DMS to DMSO and allows *Rhodovulum sulfidophilum* to grow under photolithotrophic conditions with DMS as the electron donor. The enzyme is a 164 kDa heterotrimer composed of an α-subunit that binds a bis(molybdopterin guanine dinucleotide)Mo cofactor, a polyferredoxin β-subunit, and a γ-subunit that contains a *b*-type heme. In this study, we describe the thermodynamic characterization of the redox centers within DMS dehydrogenase using EPR- and UV−visible-monitored potentiometry. Our results are compared with those of other bacterial Mo enzymes such as NarGHI nitrate reductase, selenate reductase, and ethylbenzene dehydrogenase. A remarkable similarity in the redox potentials of all Fe−S clusters is apparent.

The superfamily of molybdenum oxotransferase and hydroxylase enzymes comprises three distinct families that can be distinguished by the structure of the enzyme active site (*1*). These are the DMSO[1] reductase family, the sulfite oxidase family, and the xanthine oxidase family. Structural studies have revealed that enzymes of the DMSO reductase family share an active site comprising a molybdenum ion coordinated to two bidentate pterin dithiolene (molybdopterin) ligands (Figure 1). In most, but not all, cases, an oxo/hydroxo ligand and an amino acid side chain complete the first coordination sphere. So far, this amino acid ligand has been found to be cysteine, selenocysteine, aspartate, or serine (*2*).

Nearly all mononuclear Mo enzymes investigated to date catalyze hydride or oxygen atom transfer reactions in either the oxidative or reductive direction as generalized by eq 1. They utilize a wide variety of substrates, including sulfoxides, oxoanions, hydrocarbons, aldehydes, and tertiary amine oxides, depending on the enzyme.

$$X + H_2O \rightleftharpoons XO + 2H^+ + 2e^- \quad (1)$$

Molybdoenzymes from the DMSO reductase family have been found in only prokaryotes, and more than 15 examples

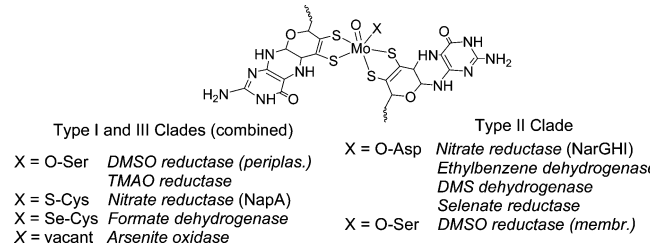

FIGURE 1: Mo cofactor in enzymes of the DMSO reductase family.

have been characterized so far from the bacteria and archaea; however, hundreds more have been identified from genomic sequencing (*3*). Enzymes of this family constitute the most diverse of all in function, and they have a key role in the biogeochemical cycling of a number of elements, including nitrogen, sulfur, arsenic, and selenium (*4, 5*). The subject of this study, DMS dehydrogenase, catalyzes the oxidation of DMS to DMSO. DMS is a major organosulfur compound found in the marine environment, and the production, consumption, and sea−atmosphere exchange of this compound have been proposed to exert an important effect on cloud formation and, hence, climate control (*6*). DMS dehydrogenase has been isolated from *Rhodovulum sulfidophilum*, a marine purple photosynthetic bacterium that can grow photoautotrophically with DMS as the sole electron donor (*7*). This periplasmic enzyme catalyzes the oxidation of DMS to DMSO, providing electrons to the photochemical reaction center in a reaction that is mediated by cytochrome c_2 (*8, 9*).

Protein phylogeny of the DMSO reductase family has revealed evolutionary relationships between enzymes which can be divided into a number of clades. A comprehensive review of this area has appeared (*3*), which also illustrates the vast number of novel bacterial Mo enzymes from this group recently identified from genomic sequencing. This information based on polypeptide primary structure has been

[†] This work was supported by Australian Research Council Discovery Grants to P.V.B. and A.G.M. (DP0343405) and G.R.H. (DP0453050) as well as a University of Queensland Graduate School Scholarship to N.L.C.

* To whom correspondence should be addressed. E-mail: p.bernhardt@uq.edu.au. Phone: +61 7 3365 4266. Fax: +61 7 3365 4299.

[‡] School of Molecular and Microbial Sciences.

[§] Centre for Magnetic Resonance.

[1] Abbreviations: DMS, dimethylsulfide; DMSO, dimethylsulfoxide; EPR, electron paramagnetic resonance; NOTA, 1,4,7-triazacyclononane triacetate; EDTA, ethylenediaminetetraacetate; AMMMEsar, 1-amino-8-methyl-3,6,10,13,16,19-hexaazabicyclo[6.6.6]eicosane; diammac, 6,13-dimethyl-1,4,8,11-tetraazacyclotetradecane-6,13-diamine; NHE, normal hydrogen electrode.

10.1021/bi702444r CCC: $40.75
Published on Web 02/26/2008

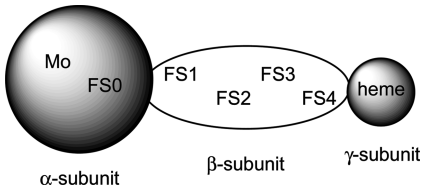

FIGURE 2: Spatial organization of the redox cofactors defining the direction of electron flow in DMS dehydrogenase (not to scale). The α- and *β*-subunits are conserved across the type II clade enzymes from the DMSO reductase family.

augmented by protein structural information derived from X-ray crystal structures. The type II clade includes the membrane-bound nitrate reductase (NarGHI) (*10, 11*), selenate reductase (*5, 12*), ethylbenzene dehydrogenase (*13–15*), and DMS dehydrogenase (*8, 16*). All enzymes within this subgroup appear to share a common active site comprising two molybdopterin ligands, a single aspartate side chain, and an oxo ligand in their fully oxidized (Mo^{VI}) state (Figure 1).

Enzymes from the type II clade contain three subunits, two of which are highly homologous. The α-subunit contains the Mo active site and, in addition, a novel (3-Cys, 1-His coordinated) $[4Fe\text{-}4S]^{2+/+}$ cluster (FS0) that for many years had escaped detection until crystallographic characterization of NarGH(I) nitrate reductase (*10, 11*). Subsequently, EPR spectroscopy was used to detect this unusual high-spin Fe−S center in its reduced form (*17*). The adjacent *β*-subunit contains four Fe−S clusters. One is a $[3Fe\text{-}4S]^{+/0}$ cluster (FS4), while the other three are $[4Fe\text{-}4S]^{2+/+}$ clusters (FS1−FS3) that act as an electron relay during catalysis. There is diversity in the third subunit associated with type II enzymes. Nitrate reductase possesses a diheme *b*-type cytochrome which is an integral membrane protein that is involved in the oxidation of quinol. The details of the assembly of the cofactor within this complex enzyme have recently been reported (*18*). In contrast, the other enzymes of the type II clade (ethylbenzene dehydrogenase, selenate reductase, and DMS dehydrogenase) possess a monomeric *b*-type cytochrome (*γ*-subunit) and are periplasmic water-soluble enzymes.

If the mechanism of catalysis in DMS dehydrogenase follows that of other Mo enzymes (*1*), the active site should cycle between its Mo^{IV} and Mo^{VI} oxidation states. Substrate binding to an oxo−Mo^{VI} (O═Mo^{VI}) active site is accompanied by a coupled two-electron, two-proton, O-atom transfer (from the O═Mo^{VI} group to DMS) in the reductive half-reaction. Electrons deposited on the Mo ion (now in its Mo^{IV} oxidation state) are then passed, via the five intervening Fe−S clusters in the α- and *β*-subunits, to the *b*-type heme in the *γ*-subunit. This heme ultimately is reoxidized by its electron acceptor (cytochrome c_2), which in turn donates electrons to the photosynthetic reaction center (*8*). Interestingly, despite their strong structural similarity and the conservation of their redox centers, some enzymes from the type II clade are reductases while others are dehydrogenases. In the reductases, electrons flow from an electron donor to the *γ*-subunit to the *β*-subunit to the α-subunit, where they are consumed by the substrate, while in the dehydrogenases, electrons ensuing from substrate oxidation flow from the α-subunit to the *β*-subunit to the *γ*-subunit (Figure 2). The enzymes of this clade represent an interesting example of how nature organizes long-range electron transfer across several redox centers seemingly with the same (or similar) apparatus yet for entirely different purposes. In this study, we have determined the potentials of the redox centers from all three subunits within DMS dehydrogenase using spectropotentiometric (EPR and optical) methods. The data are compared with those of other enzymes from the type II clade.

EXPERIMENTAL PROCEDURES

Reagents. All reagents were obtained commercially and used without further purification, except for Tricine buffer, which was purified by being passed through a Chelex column to remove traces of metal ions.

Enzyme Preparation. DMS dehydrogenase was isolated from wild-type *Rv. sulfidophilum* strain SH1 as previously described (*9, 16*).

Redox Potentiometry. Potentials for all experiments were measured with a combination Pt wire−Ag/AgCl electrode attached to a Hanna 8417 meter. The electrode was calibrated against a saturated solution of quinhydrone [$E^{\circ\prime}$(pH 7) = 284 mV vs NHE]. All samples were titrated inside a Belle Technology anaerobic box (<10 ppm O_2).

(1) Optical Potentiometry Experiments. The heme redox potential of native DMS dehydrogenase was determined by standard optical redox potentiometric techniques (*19, 20*), using the Soret bands of the chromophores as the indicator of reduction. The mediators used were Fe(NOTA) ($E_{m,7}$ = 214 mV) and Na[Fe(EDTA)] ($E_{m,7}$ = 98 mV), each present at a concentration of 50 *μ*M as described previously (*21*). The enzyme concentration was 5 *μ*M in 20 mM Tris-HCl (pH 8). All measurements were taken within a glovebox under an atmosphere of N_2 using a Shimadzu UV Mini 1240 spectrophotometer with the spectrochemical cell thermostated at 25 °C. The potential was altered using $Na_2S_2O_4$ (100 mM) and $K_2S_2O_8$ (100 mM) as the reductant and oxidant, respectively.

The heme midpoint potential (E_m) was calculated from eq 2, a combination of the Beer–Lambert and Nernst equations for a single electron redox couple (ox + e^- → red) involving two absorbing species at 298 K (*21*).

$$A = \frac{A_{ox} \times 10^{(E-E_m)/59} + A_{red}}{10^{(E-E_m)/59} + 1} \quad (2)$$

In this case, A is the absorbance at 424 nm, A_{red} and A_{ox} are the limiting absorbance of the ferrous and ferric heme chromophores at the same wavelength, respectively, and E is the observed potential.

(2) EPR Experiments. The $Mo^{V/IV}$ and $Mo^{VI/V}$ redox potentials were determined using EPR-monitored potentiometry of solutions frozen at 120 K. The DMS dehydrogenase concentration was 20 *μ*M in pH 8 Tricine (50 mM), which was chosen to minimize pH changes upon freezing (*22*). All mediators were present at a final concentration of 50 *μ*M. The mediators used were diaminodurol ($E_{m,7}$ = 276 mV), dichlorophenolindophenol ($E_{m,7}$ = 217 mV), 2,6-dimethylbenzoquinone ($E_{m,7}$ = 180 mV), phenazine methosulfate ($E_{m,7}$ = 80 mV), 2,5-dihydroxybenzoquinone ($E_{m,7}$ = −60 mV), 2-hydroxy-1,4-naphthoquinone ($E_{m,7}$ = −152 mV), and anthroquinone-2-sulfonic acid ($E_{m,7}$ = −225 mV). The reductant was $Na_2S_2O_4$ (100 mM), and $K_3[Fe(CN)_6]$ (100 mM) was used as the oxidant. Each sample (300 *μ*L) was poised at a particular potential (within a glovebox), then

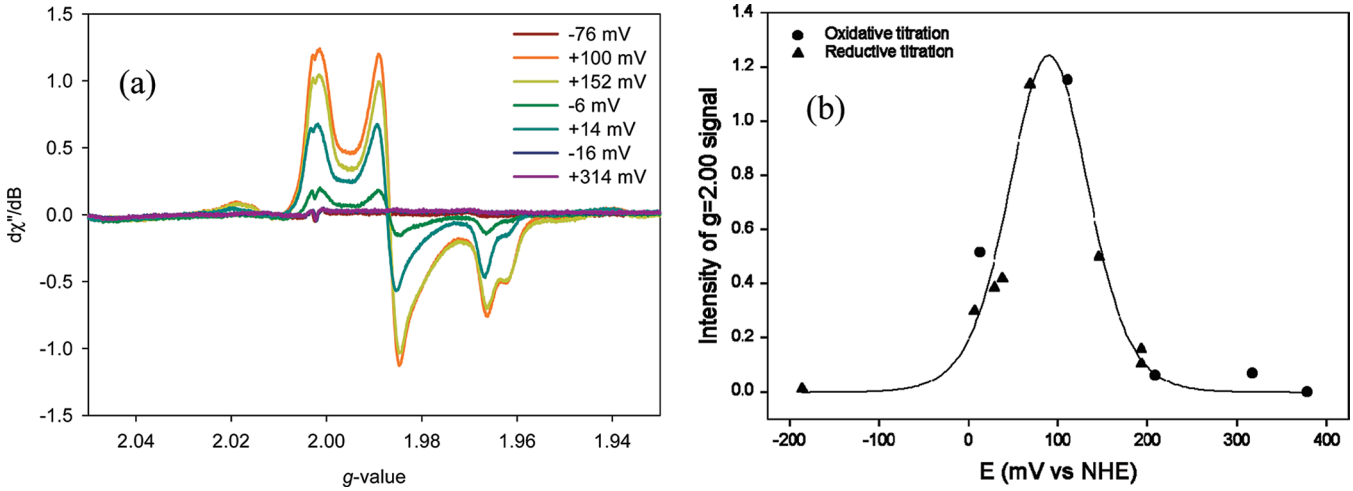

FIGURE 3: (a) EPR redox titration of the Mo^V signal of DMS dehydrogenase (120 K). See Experimental Procedures for conditions. (b) Variation in the Mo^V EPR $g = 1.99$ signal intensity of DMS dehydrogenase as a function of redox potential. The calculated curve (eq 3) is shown for redox potentials of 55 ± 10 mV ($Mo^{IV/V}$) and 123 ± 13 mV ($Mo^{V/VI}$).

sealed in a 3 mm internal diameter quartz EPR tube, and immediately frozen in liquid nitrogen. Continuous wave X-band (ca. 9.3 GHz) EPR spectra were recorded with a Bruker Biospin Elexsys E580 EPR spectrometer fitted with a super high Q cavity. Calibration of the magnetic field and microwave frequency was achieved with a Bruker ER 036TM Teslameter and a Bruker microwave frequency counter, respectively. A microwave power of 20 mW was used. A flow-through cryostat in conjunction with a Eurotherm (B-VT-2000) variable-temperature controller provided temperatures of 127–133 K at the sample position in the cavity. For lower temperatures (1.7–5 K), an Oxford Instruments ESR 910 flow-through cryostat in conjunction with an ITC503 temperature controller was employed. Spectrometer tuning, signal averaging, and visualization were done with Bruker's Xepr (version 2.4b.12). The intensity of the Mo^V signal (I) was recorded as a function of potential (E).

$$I = \frac{I_{max}}{1 + 10^{(E-E_1)/59} + 10^{(E_2-E)/59}} \quad (3)$$

The experimental data were fit to eq 3, where E_1 is the potential of the $Mo^{VI/V}$ couple, E_2 is the potential of the $Mo^{V/IV}$ couple, and I_{max} is the maximum EPR intensity (proportional to the maximum amount of Mo^V formed at the midpoint of the titration) (*21*). Note that the temperature at which the sample is equilibrated (298 K) prior to freezing still applies in this Nernst relationship as the system is equilibrated at this temperature.

For determination of the redox potentials of the Fe−S clusters in the β-subunit of DMS dehydrogenase (FS1−FS4), EPR redox potentiometry at very low temperatures was necessary to compensate for the much shorter relaxation times inherent to these paramagnetic centers. The enzyme concentration was 30 μM, and all measurements were taken in 20 mM Tricine (pH 8). The mediators used in this experiment are as described above for Mo potentiometry, with the addition of three coordination compounds, $[Co(AMMEsar)]^{3+/2+}$ ($E_{m,7} = -378$ mV), $[Co(cis\text{-diammac})]^{3+/2+}$ ($E_{m,7} = -500$ mV), and $[Co(trans\text{-diammac})]^{3+/2+}$ ($E_{m,7} = -555$ mV), described elsewhere (*21*) at a concentration of 25 μM to avoid problems with enzyme precipitation. The reductant was $Na_2S_2O_4$ (or Ti^{III} citrate for potentials below −400 mV vs NHE), while the oxidant was $Na_2S_2O_8$ (all at concentrations of ~5 mM). The samples were titrated to the desired potential as described above before being transferred to EPR tubes (sealed in a glovebox) and frozen in liquid N_2. Each sample was analyzed by EPR at 2 K. The FS4 cluster is EPR active in its oxidized $[3Fe\text{-}4S]^+$ form only while the FS1−FS3 centers become EPR active only upon reduction to the $[4Fe\text{-}4S]^+$ form. The signals observed from each center were titrated in the reducing and oxidizing directions as described above, and data were analyzed with eq 2 where the EPR intensities replace the optical absorbance values.

RESULTS AND DISCUSSION

Mo Active Site. The $Mo^{V/IV}$ and $Mo^{VI/V}$ redox potentials of DMS dehydrogenase were determined by using EPR spectroscopy at pH 8 by monitoring formation and decay of the Mo^V EPR signal as a function of redox potential. The rhombic ($g = 1.99$, 1.98, and 1.96) Mo^V EPR spectrum of DMS dehydrogenase has been reported previously (*16*) and shows no resolved hyperfine coupling. The coordination sphere of the Mo ion is believed to include an aqua ligand at this pH as discussed previously (*16*) in addition to the four S donors of the two bidentate molybdopterins. On the basis of sequence similarity with other structurally characterized enzymes, NarGH nitrate reductase (*10, 11*) and ethylbenzene dehydrogenase (*14*), it is likely that an aspartate residue is also coordinated to the Mo ion in DMS dehydrogenase.

As seen in Figure 3a, the Mo^V signal grows and is maximal at ca. 100 mV. The midpoint redox potentials were found to be 55 ± 10 and 123 ± 13 mV vs NHE for the $Mo^{V/IV}$ and $Mo^{VI/V}$ couples, respectively (Figure 3b). The features of the molybdenum EPR spectra arising from DMS dehydrogenase under various experimental conditions (pH, coordinating anions) have been discussed elsewhere (*16*). The reversibility of the titration is apparent from Figure 3b, where the oxidative (●) and reductive (▲) parts of the titration are indicated by different symbols.

Iron−Sulfur Clusters. Of the five iron−sulfur clusters predicted to be present in DMS dehydrogenase (FS0 in the α-subunit and FS1−FS4 in the β-subunit), four (FS1−FS4) were observed spectroscopically in this work, and their redox

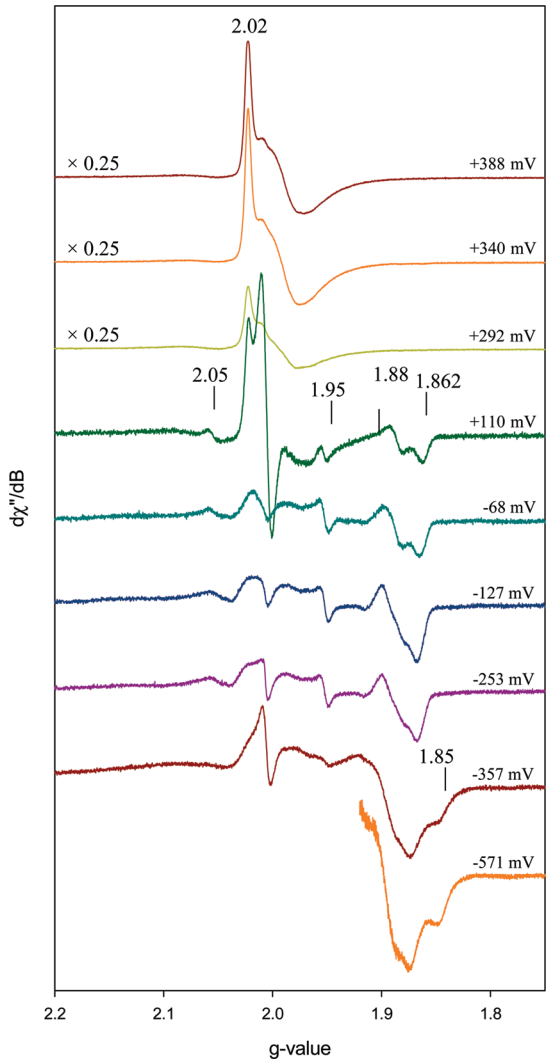

FIGURE 4: Variation in the Fe−S EPR signals (FS1−FS4) as a function of redox potential ($T = 2$ K). Note the change of scale to compensate for the intense FS4 signal at high potential. At 110 mV, an intense Mo^V signal is apparent at $g = 2.00$ and the Ti^{III}(citrate) resonance around $g = 2.0$ has been omitted from the lowest-potential spectrum.

potentials have been determined. Note that the assignment of each center has been possible by analogy with the comprehensive and systematic studies on both the β-subunits of nitrate reductase (NarH) and DMSO reductase (DmsB) (*17, 23, 25–27*), where site-directed mutagenesis and EPR redox potentiometry enabled the assignment of all Fe−S clusters to their associated EPR signals. The EPR spectra of the Fe−S clusters of DMS dehydrogenase are sufficiently similar that they can be assigned by analogy. The conventional numbering of the clusters is according to their sequential position within the enzyme, FS0 being closest to the Mo ion and FS4 being closest to the heme (Figure 2). Previously published EPR experiments with DMS dehydrogenase (*16*) revealed the presence of a $[3Fe\text{-}4S]^{+/0}$ cluster and several $[4Fe\text{-}4S]^{2+/+}$ clusters, as anticipated from homology with other type II enzymes from this clade, including nitrate reductase and ethylbenzene dehydrogenase.

The EPR spectra of the Fe−S centers in the β-subunit of DMS dehydrogenase at 2 K as a function of redox potential are presented in Figure 4, and the data analysis is shown in Figure 5a−d, including the theoretical curves derived from a fit to eq 2 in each case. A summary of all redox potentials determined here potentiometrically is given in Table 1 in comparison with the data from other type II clade enzymes from the DMSO reductase family, and the relevant g values are listed in Table 2.

Each Fe−S cluster observed here (FS1–FS4) gives a characteristic set of signals as seen before for the well-studied NarH subunit of nitrate reductase (*17, 25–27*). The $[4Fe\text{-}4S]^+$ clusters exhibit a rhombic signal with three well-separated g values (Table 2), while the most intense signal is provided by the $[3Fe\text{-}4S]^+$ cluster (FS4) and is most apparent in the EPR spectrum of the fully oxidized enzyme (Figure 4, top spectrum). The $g = 2.02$ signal titrates to zero intensity as the potential is lowered (Figure 5d), and a redox potential of 292 mV versus NHE was determined for FS4.

Further reduction of the sample gives rise to spectra with features appearing in the $g = 2.05$, 1.95, 1.88, and 1.86 region (Figure 4). These features are very similar to those seen before in the NarH subunit (FS1–FS4) of nitrate reductase (*17, 25–27*). The $g = 1.862$ signal from reduced FS1 was monitored to determine its redox potential [175 mV (Figure 5a)] followed by the FS3 center at $g = 1.95$ [66 mV (Figure 5c)]. The last center (FS2) is reduced at a much lower potential, and the redox potential was determined in two ways. As the sample is reduced to low potential, the $g = 1.862$ peak shifts gradually to a $g = 1.87$ peak, while the $g = 1.95$ and 2.05 signals fade at very low potentials. It is not clear what interactions among the four clusters cause the disappearance of these signals, both from the same cluster, at lower potentials in DMS dehydrogenase, but dipole–dipole coupling between nearby electron spins must be occurring. The growth of the $g = 1.85$ signal (Figure 5b) coincided with disappearance of the $g = 1.95$ or $g = 2.05$ signal, leading to a redox potential for the FS2 center of −337 mV.

Although no structural data for DMS dehydrogenase are available at this time, a further $[4Fe\text{-}4S]^{2+/+}$ cluster (FS0) should reside in the α-subunit (adjacent to the Mo cofactor), as determined from sequence similarity with the structurally characterized NarG subunit (*10, 11, 28*) and ethylbenzene dehydrogenase (*14*). On the basis of structural (*10, 11, 28*) and EPR spectroscopic work (*17*) with NarG, the FS0 cluster should contain a high-spin center bearing three coordinating cysteine ligands and one coordinating histidine ligand (*17*). Although the incidence of high-spin ($S = {}^3/_2$) iron−sulfur clusters is uncommon, and consequences for having this unusual spin state are poorly understood, they almost invariably involve a non-cysteinyl coordinating amino acid (*17*). The only EPR evidence for this cluster in any related enzyme has been found for NarG, in which a low field signal is observed only at high power and low temperature (*17*). Similar experimental EPR conditions were explored here with DMS dehydrogenase, but we have yet to obtain convincing evidence for a signal characteristic of the FS0 center. We can be sure that the Mo cofactor is present (in the α-subunit where the FS0 cofactor should also reside) as the Mo^V signal is seen clearly in the 120 K EPR spectra (Figure 3a) and also at 2 K (Figure 4, 110 mV spectrum). On this basis, the α-subunit appears to have been properly assembled with its putative FS0 center (*18*). It is worth mentioning that the FS0 center remained undetected by EPR for many years until it was revealed by the recent crystal structures of NarGH(I) nitrate reductase (*10, 11, 28*)

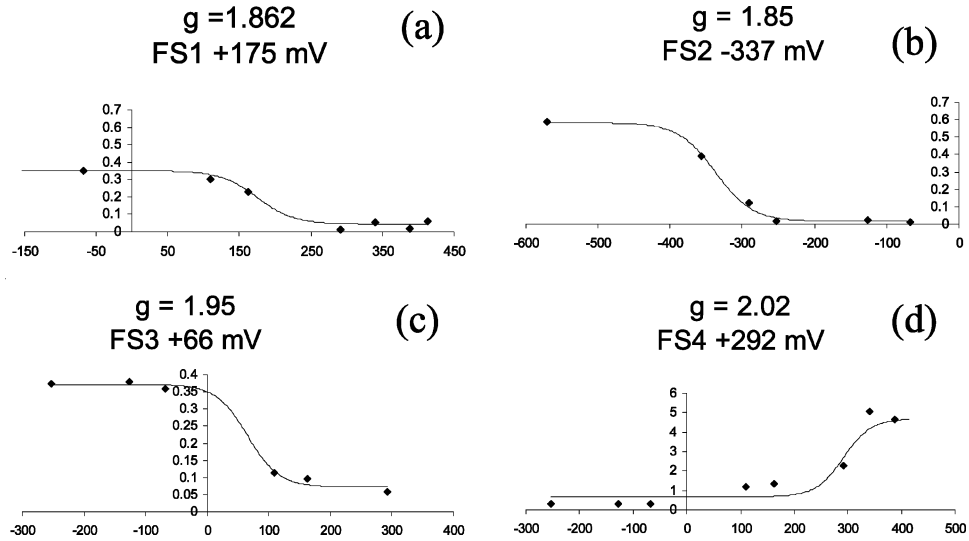

FIGURE 5: EPR intensities from the (a) FS1 center, (b) FS2 center, (c) FS3 center, and (d) FS4 center as a function of redox potential (mv vs NHE).

Table 1: Redox Potentials (millivolts vs NHE) of Type II Clade Enzymes from the DMSO Reductase Family (*17*)

	α-subunit			β-subunit				γ-subunit
enzyme (ref)	$Mo^{V/IV}$	$Mo^{VI/V}$	FS0 $[4Fe\text{-}4S]^{+}$	FS1 $[4Fe\text{-}4S]^{+}$	FS2 $[4Fe\text{-}4S]^{+}$	FS3 $[4Fe\text{-}4S]^{+}$	FS4 $[3Fe\text{-}4S]^{+}$	heme(s)
DMS dehydrogenase (this work)	+55	+123	nd[a]	+175 (±20)	−337 (±20)	+66 (±20)	+292 (±20)	+324 (±20)
nitrate reductase (*17*)	+130	+205	−55	+130	−420	−55	+180	+20, +120
DMSO reductase (*23*)	−175	−15	nd[a]	−120	−330	−50	−240	−
ethylbenzene dehydrogenase (*24*)	+80	+225	nd[a]	−15	−400	−8	+70	+255
selenate reductase (*5*)	nd[a]	nd[a]	nd[a]	+183	−356	−51	+118	nd[a]

[a] Centers not determined.

Table 2: EPR-Derived *g* Values of the Rhombic Fe−S Clusters in the β-Subunit of DMS Dehydrogenase

g value	FS1	FS2	FS3	FS4
g_1	1.862	1.851	1.867	1.965
g_2	1.887	1.897	1.852	1.987
g_3	2.016	2.015	2.050	2.018

and ethylbenzene dehydrogenase (*14*). These structural studies provided the impetus for spectroscopic studies in search of a center that evidently can be observed only by EPR under special conditions.

Heme b Cofactor. The midpoint potential of the *b*-type heme in the γ-subunit of DMS dehydrogenase was determined by optical redox potentiometry using the coordination compounds Fe(NOTA) and $[Fe(EDTA)]^{-}$ as mediators. In this case, the intense ferric and ferrous heme absorption spectra are dominant and the other redox centers do not interfere. The data are presented in Figure 6, and the resulting heme redox potential (324 ± 20 mV vs NHE, an average of three titrations) is in agreement with the potential previously published using a different set of (organic) redox mediators (315 ± 20 mV vs NHE) (*16*).

The crystal structure of the highly homologous ethylbenzene dehydrogenase reveals a novel lysine/methionine axial ligation in the corresponding *b*-type heme (*14*), and it is likely that the same ligands are involved in coordinating the heme cofactor in DMS dehydrogenase on the basis of homology modeling. These same lysine and methionine residues are indeed conserved in the sequences of the γ-subunits of ethylbenzene dehydrogenase, DMS dehydrogenase, and selenate reductase (*14*). There is genetic evidence (*8*) that the electron acceptor for DMS dehydrogenase is a cytochrome c_2, with a redox potential of 357 mV versus NHE (*29*). The high redox potential of the heme *b* cofactor, coupled with the even higher redox potential of its electron acceptor, is consistent with the proposal that the *b*-type cytochrome in DMS dehydrogenase is the site of electron egress from the enzyme in a pathway of electron flow to the oxidized bacteriochlorophyll special pair of the photosynthetic reaction center.

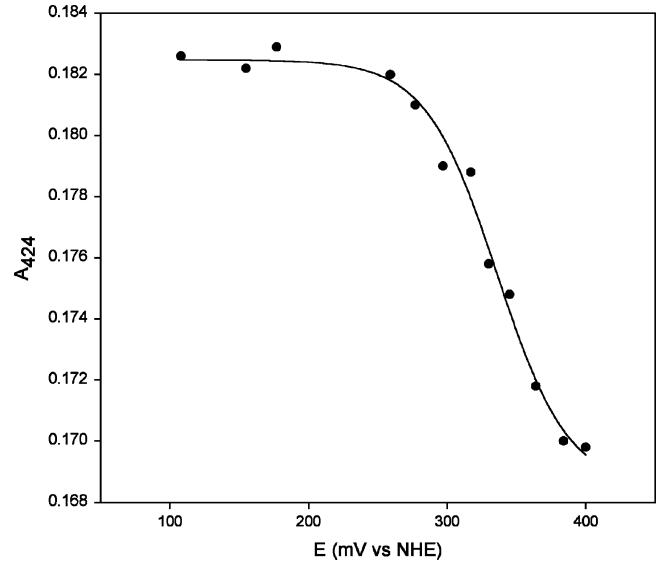

FIGURE 6: Optical potentiometric redox titration of the heme cofactor in DMS dehydrogenase. The intensity of the Soret band of the Fe^{II} form (at 424 nm) is shown as a function of potential, and the calculated curve obtained from a fit to eq 2 is shown.

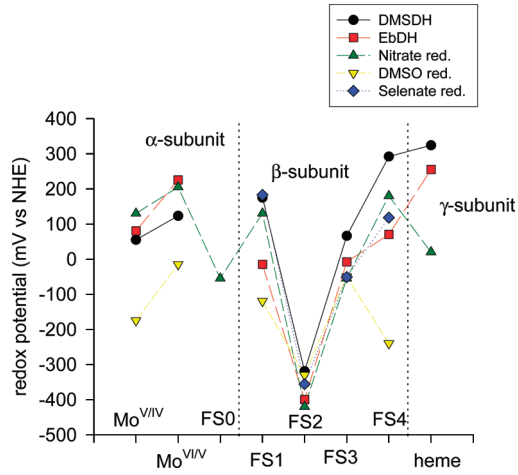

FIGURE 7: Graphical illustration of redox potentials of the cofactors in order of their spatial organization within type II clade enzymes from the DMSO reductase family.

CONCLUSIONS

Despite their diverse function, enzymes from the type II clade of the DMSO reductase family exhibit an interesting similarity in their architecture and even the redox potentials of some cofactors. Figure 7 illustrates the variations in redox potential along the electron transport chain where each cofactor shown is involved due to its physical location within the enzyme. Without any one of the redox centers in the α- and β-subnuits, the distance for electron transfer becomes prohibitively large (*30*), so all must be engaged at some point in electron transfer during turnover. An interesting feature is the presence of the very low potential center FS2 in all enzymes. It may be viewed as a bottleneck in electron egress from the Mo active site to the γ-subunit in the dehydrogenases and in electron flow to the Mo active site in the reductases. In any case, the thermodynamics of the overall enzyme reaction are driven by the substrate redox potential (not usually known accurately) and the potential of the redox partner (which acts as an electron acceptor or electron donor, depending on the direction of the oxidation–reduction process). In other words, the centers shown in Figure 7 constitute only a "wire" through which the overall exergonic electron transfer process is conducted. The redox potentials we report here are an important foundation for our continuing investigations into the catalytic activity of DMS dehydrogenase.

ACKNOWLEDGMENT

We gratefully acknowledge Dr. Simon Drew for assistance with spectroscopic measurements and Dr. Ulrike Kappler for valuable discussions.

REFERENCES

1. Hille, R. (1996) The Mononuclear Molybdenum Enzymes. *Chem. Rev. 96*, 2757–2816.
2. McEwan, A. G., Kappler, U., and McDevitt, C. A. (2004) Microbial molybdenum-containing enzymes in respiration: Structural and functional aspects. *Adv. Photosynth. Respir. 15*, 175–202.
3. Rothery, R. A., Workun, G. J., and Weiner, J. H. (2007) The prokaryotic complex iron-sulfur molybdoenzyme family. *Biochim. Biophys. Acta,* doi: 10.1016/j.bbamem.2007.1009.1002.
4. Stolz, J. F., Basu, P., Santini, J. M., and Oremland, R. S. (2006) Arsenic and selenium in microbial metabolism. *Annu. Rev. Microbiol. 60*, 107–130.
5. Dridge, E. J., Watts, C. A., Jepson, B. J. N., Line, K., Santini, J. M., Richardson, D. J., and Butler, C. S. (2007) Investigation of the redox centres of periplasmic selenate reductase from *Thauera selenatis* by EPR spectroscopy. *Biochem. J. 408*, 19–28.
6. Bopp, L., Aumont, O., Belviso, S., and Monfray, P. (2003) Potential impact of climate change on marine dimethyl sulfide emissions. *Tellus, Ser. B 55*, 11–22.
7. Hanlon, S. P., Holt, R. A., Moore, G. R., and McEwan, A. G. (1994) Isolation and characterization of a strain of *Rhodobacter sulfidophilus*: A bacterium which grows autotrophically with dimethylsulfide as electron donor. *Microbiology 140*, 1953–1958.
8. McDevitt, C. A., Hugenholtz, P., Hanson, G. R., and McEwan, A. G. (2002) Molecular analysis of dimethyl sulphide dehydrogenase from *Rhodovulum sulfidophilum*: Its place in the dimethyl sulphoxide reductase family of microbial molybdopterin-containing enzymes. *Mol. Microbiol. 44*, 1575–1587.
9. Hanlon, S. P., Toh, T.-H., Solomon, P. S., Holt, R. A., and McEwan, A. G. (1996) Dimethylsulfide:acceptor oxidoreductase from *Rhodobacter sulfidophilus*. The purified enzyme contains *b*-type heme and a pterin molybdenum cofactor. *Eur. J. Biochem. 239*, 391–396.
10. Bertero, M. G., Rothery, R. A., Palak, M., Hou, C., Lim, D., Blasco, F., Weiner, J. H., and Strynadka, N. C. J. (2003) Insights into the respiratory electron transfer pathway from the structure of nitrate reductase A. *Nat. Struct. Biol. 10*, 681–687.
11. Jormakka, M., Richardson, D., Byrne, B., and Iwata, S. (2004) Architecture of NarGH Reveals a Structural Classification of MobisMGD Enzymes. *Structure 12*, 95–104.
12. Schroder, I., Rech, S., Krafft, T., and Macy, J. M. (1997) Purification and characterization of the selenate reductase from *Thauera selenatis*. *J. Biol. Chem. 272*, 23765–23768.
13. Kniemeyer, O., and Heider, J. (2001) Ethylbenzene dehydrogenase, a novel hydrocarbon-oxidizing molybdenum/iron-sulfur/heme enzyme. *J. Biol. Chem. 276*, 21381–21386.
14. Kloer, D. P., Hagel, C., Heider, J., and Schulz, G. E. (2006) Crystal structure of ethylbenzene dehydrogenase from *Aromatoleum aromaticum*. *Structure 14*, 1377–1388.
15. Szaleniec, M., Hagel, C., Menke, M., Nowak, P., Witko, M., and Heider, J. (2007) Kinetics and Mechanism of Oxygen-Independent Hydrocarbon Hydroxylation by Ethylbenzene Dehydrogenase. *Biochemistry 46*, 7637–7646.
16. McDevitt, C. A., Hanson, G. R., Noble, C. J., Cheesman, M. R., and McEwan, A. G. (2002) Characterization of the Redox Centers in Dimethyl Sulfide Dehydrogenase from *Rhodovulum sulfidophilum*. *Biochemistry 41*, 15234–15244.
17. Rothery, R. A., Bertero, M. G., Cammack, R., Palak, M., Blasco, F., Strynadka, N. C. J., and Weiner, J. H. (2004) The catalytic subunit of *Escherichia coli* nitrate reductase A contains a novel [4Fe-4S] cluster with a high-spin ground state. *Biochemistry 43*, 5324–5333.
18. Lanciano, P., Vergnes, A., Grimaldi, S., Guigliarelli, B., and Magalon, A. (2007) Biogenesis of a Respiratory Complex Is Orchestrated by a Single Accessory Protein. *J. Biol. Chem. 282*, 17468–17474.
19. Dutton, P. L. (1978) Redox potentiometry: Determination of midpoint potentials of oxidation-reduction components of biological electron-transfer systems. *Methods Enzymol. 54*, 411–435.
20. Wilson, G. S. (1978) Determination of oxidation-reduction potentials. *Methods Enzymol. 54*, 396–410.
21. Bernhardt, P. V., Chen, K.-I., and Sharpe, P. C. (2006) Transition Metal Complexes as Mediator Titrants in Protein Redox Potentiometry. *J. Biol. Inorg. Chem. 11*, 930–936.
22. Williams-Smith, D. L., Bray, R. C., Barber, M. J., Tsopanakis, A. D., and Vincent, S. P. (1977) Changes in apparent pH on freezing aqueous buffer solutions and their relevance to biochemical electron-paramagnetic-resonance spectroscopy. *Biochem. J. 167*, 593–600.
23. Rothery, R. A., Trieber, C. A., and Weiner, J. H. (1999) Interactions between the molybdenum cofactor and iron-sulfur clusters of *Escherichia coli* dimethyl sulfoxide reductase. *J. Biol. Chem. 274*, 13002–13009.
24. Hagel, C. (2006) Ph.D. Thesis, Technical University of Darmstadt, Darmstadt, Germany.
25. Augier, V., Asso, M., Guigliarelli, B., More, C., Bertrand, P., Santini, C.-L., Blasco, F., Chippaux, M., and Giordano, G. (1993) Removal of the high-potential iron-sulfur [4Fe-4S] center of the β-subunit from *Escherichia coli* nitrate reductase. Physiological, biochemical, and EPR characterization of site-directed mutated enzymes. *Biochemistry 32*, 5099–5108.

26. Guigliarelli, B., Magalon, A., Asso, M., Bertrand, P., Frixon, C., Giordano, G., and Blasco, F. (1996) Complete Coordination of the Four Fe-S Centers of the β-Subunit from *Escherichia coli* Nitrate Reductase. Physiological, Biochemical, and EPR Characterization of Site-Directed Mutants Lacking the Highest or Lowest Potential [4Fe-4S] Clusters. *Biochemistry 35*, 4828–4836.
27. Guigliarelli, B., Asso, M., More, C., Augier, V., Blasco, F., Pommier, J., Giordano, G., and Bertrand, P. (1992) EPR and redox characterization of iron-sulfur centers in nitrate reductases A and Z from *Escherichia coli*. Evidence for a high-potential and a low-potential class and their relevance in the electron-transfer mechanism. *Eur. J. Biochem. 207*, 61–68.
28. Bertero, M. G., Rothery, R. A., Boroumand, N., Palak, M., Blasco, F., Ginet, N., Weiner, J. H., and Strynadka, N. C. J. (2005) Structural and biochemical characterization of a quinol binding site of *Escherichia coli* nitrate reductase A. *J. Biol. Chem. 280*, 14836–14843.
29. Yoshida, M., Masuda, S., Nagashima, K. V. P., Vermeglio, A., Shimada, K., and Matsuura, K. (2001) *In vitro* and *in vivo* electron transfer to the triheme cytochrome subunit bound to the photosynthetic reaction center complex in the purple bacterium *Rhodovulum sulfidophilum*. *Biochim. Biophys. Acta 1506*, 23–30.
30. Moser, C. C., Keske, J. M., Warncke, K., Farid, R. S., and Dutton, P. L. (1992) Nature of biological electron transfer. *Nature 355*, 796–802.

BI702444R